indistinguishable in numerical work, although they may in fact have quite different behaviors: consider orbits such as those above, whose initial conditions end with 4 and 6, respectively, in the $(N + 1)$st decimal place. We shall return to this feature subsequently, when we discuss symbolic dynamics and the shift automorphism on symbol sequences in Chapter 5.

In summary, in our sketch of the van der Pol system we have seen how the relatively simple planar phase portrait of the unforced system gives way to the more complex picture of the Poincaré map associated with the periodically forced problem. Although one can recover an equivalent planar system by averaging in the case of weak forcing, the validity of such an analysis is limited. In the strongly forced problem, approximations again permit an effective reduction of dimension, but the one-dimensional map of the circle thus produced is noninvertible and displays remarkably complex dynamics. These observations are characteristic and will reappear in other examples.

2.2. Duffing's Equation

Duffing [1918] introduced a nonlinear oscillator with a cubic stiffness term to describe the hardening spring effect observed in many mechanical problems. Since then this equation has become, together with van der Pol's equation, one of the commonest examples in nonlinear oscillation texts and research articles. In this section we discuss a modification of the conventional Duffing equation in which the linear stiffness term is negative. Such an equation describes the dynamics of a buckled beam or plate when only one mode of vibration is considered. In particular, Moon and Holmes [1979, 1980] showed that the Duffing equation in the form

$$\ddot{x} + \delta\dot{x} - x + x^3 = \gamma \cos \omega t \tag{2.2.1}$$

provides the simplest possible model for the forced vibrations of a cantilever beam in the nonuniform field of two permanent magnets. The experimental apparatus used by Moon and Holmes is sketched in Figure 2.2.1. A slender steel beam is clamped in a rigid framework which supports the magnets. Their attractive forces overcome the elastic forces which would otherwise keep the beam straight and, in the absence of external forcing, the beam settles with its tip close to one or the other of the magnets. There is also an unstable central equilibrium position, at which the magnetic forces cancel: its existence can easily be demonstrated as a "potential barrier" separating the two domains of attraction, if the beam is carefully displaced. The simplest model for such a potential is the symmetric one-dimensional field

$$V(x) = \frac{x^4}{4} - \frac{x^2}{2}, \tag{2.2.2}$$

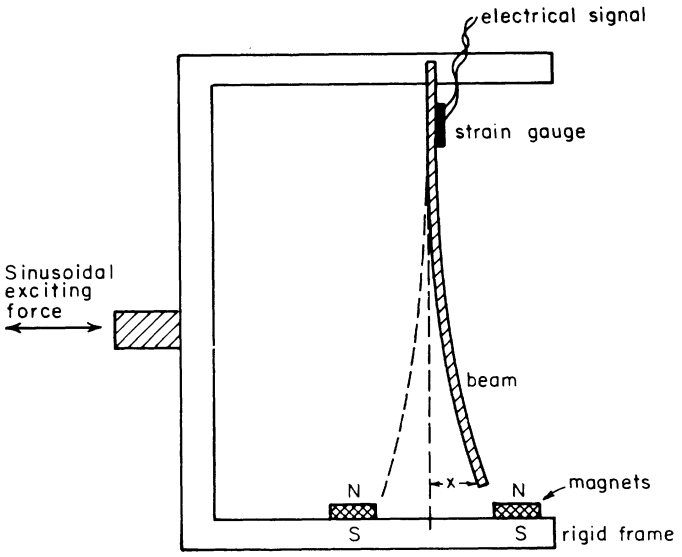

Figure 2.2.1. The magneto-elastic beam.

although the symmetry is not crucial. Here the single configuration variable x represents a characteristic measure of the beam's position, say its tip displacement. The force acting on the beam is governed by the gradient of V, and thus, using Newton's second law, a simple model for the beam is provided by

$$\ddot{x} = -\text{grad } V, \tag{2.2.3}$$

or

$$\ddot{x} - x + x^3 = 0. \tag{2.2.4}$$

The dissipation due to friction, viscous damping from the surrounding air, and magnetic damping, is modelled by a linear velocity dependent term, giving the equation

$$\ddot{x} + \delta\dot{x} - x + x^3 = 0. \tag{2.2.5}$$

Equation (2.2.5) is easy to analyze and will be found to provide a reasonable model for the motions of the beam in a stationary rigid framework. (The reader is free to add appropriate coefficients to obtain physically relevant frequencies if he wishes.) Of course, equation (2.2.5) represents only a single mode of vibration, but if the beam is sufficiently long and slender, and the magnets sufficiently powerful, vibrations *are* observed to occur primarily in the first mode (cf. Moon and Holmes [1979]).

Now we begin to shake the apparatus sinusoidally as shown, using an electromagnetic vibration generator. This is modelled by the addition of a

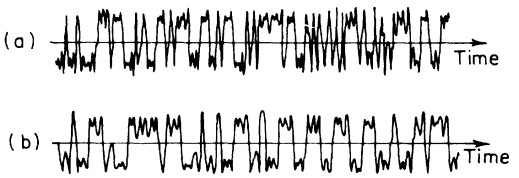

Figure 2.2.2. (a) Vibrations of the beam, and (b) a solution of equation (2.2.1).

forcing term, and thus we obtain equation (2.2.1).* In fact Moon and Holmes derived (2.2.1) as a Galerkin approximation of a set of rather general partial differential equations for an elastic beam in a nonuniform magnetic field, and a good case can be made for its relevance as the simplest possible model for the experiment. The sketch given here is only intended to make the model plausible.

An electromechanical strain gauge glued near the root of the beam measures the curvature at that point as a function of time. Since the motion is primarily in the first mode, this effectively provides a measure of the tip displacement $x(t)$. For low force amplitudes, γ, we observe periodic motions close to either one or the other magnet, but as γ is slowly increased, a point comes at which the beam "suddenly" begins whipping back and forth in an irregular, apparently chaotic manner. This is not a transient phenomenon: with γ and ω, the forcing frequency, fixed, such chaotic motions have been observed for periods of hours, or for $\approx 10^5$ cycles of the forcing function. A short piece of such a record is shown in Figure 2.2.2, together with a typical solution of (2.2.1).

The qualitative agreement is clear, although the reader may like to ponder why the experimental record is "spikier" than the solution of (2.2.1), and appears to contain higher frequency components (this spikiness is *not* a consequence of the measurement technique). We can therefore place some confidence in our simple model, which we now discuss.

We first consider the problem without external forcing $\gamma = 0$. We introduce an additional parameter β which measures the relative strength of the magnetic and elastic forces. An increase in β corresponds (approximately) to an increase in strength of the magnetic forces. The system is

$$\ddot{x} + \delta\dot{x} - \beta x + x^3 = 0,$$

or, as a first-order equation

$$\begin{aligned} \dot{u} &= v, \\ \dot{v} &= \beta u - u^3 - \delta v, \end{aligned} \tag{2.2.6}$$

and it is easy to check that, for $\beta < 0$ (weak magnets), there is a single equilibrium at $(x, \dot{x}) = 0$ while if $\beta > 0$, there are three equilibria at $x = 0$,

* Since the beam is subject to inertial excitation, for frame displacement $\Gamma \cos \omega t$ the force on the beam is actually of the form $\Gamma\omega^2 \cos \omega t$. We subsume the ω^2 in the parameter γ.

$\pm\sqrt{\beta}$. If $\delta > 0$, the equilibria are, respectively, a sink (for $\beta < 0$) and two sinks and a saddle (for $\beta > 0$). In terms of the bifurcation analyses of Chapters 3 and 7, (2.2.6) undergoes a pitchfork bifurcation of equilibria as β passes through zero.

To obtain global information on the phase portrait, we note that, for $\delta = 0$, the system is Hamiltonian with Hamiltonian energy

$$H(u, v) = \frac{v^2}{2} - \beta\frac{u^2}{2} + \frac{u^4}{4}. \tag{2.2.7}$$

Since the solutions lie on level curves of H, we can immediately draw the phase portraits for $\delta = 0$ as in Figure 2.2.3(a). Addition of the term $-\delta v$ to the second equation directs the vector field inward in all the closed level curves (except at $v = 0$) and we therefore obtain the qualitative behaviors of Figure 2.2.3(b). In particular, a closed, simply connected region $D \subset \mathbb{R}^2$ can be found such that the vector field is directed inward everywhere on its boundary. This global stability property persists even for nonzero forcing, when the vector field is time dependent (cf. Holmes [1979a], Holmes and Whitley [1983a]). We now turn to this case.

Letting $\gamma \neq 0$ and setting $\beta = 1$, we return to equation (2.2.1), which may be rewritten as an autonomous system

$$\left.\begin{aligned} \dot{u} &= v, \\ \dot{v} &= u - u^3 - \delta v + \gamma \cos \omega\theta, \\ \dot{\theta} &= 1, \end{aligned}\right\} \qquad (u, v, \theta) \in \mathbb{R}^2 \times S^1, \tag{2.2.8}$$

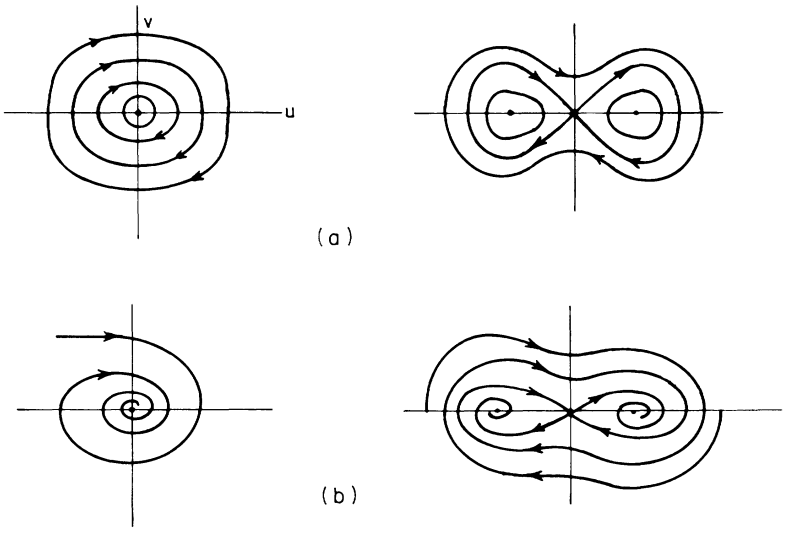

Figure 2.2.3. Duffing's equation without external forcing. (a) $\delta = 0$; (b) $\delta > 0$.

where $S^1 = \mathbb{R}/T$ is the circle of length $T = 2\pi/\omega$. We pick a cross section $\Sigma = \{(u, v, \theta) | \theta = 0\}$ and consider the Poincaré map $P: \Sigma \to \Sigma$ (the stability property referred to above, and the consequent boundedness of all solutions, ensures that P is globally defined). Clearly, P depends upon the parameters γ, δ, ω, but in what follows we shall take δ and ω as fixed, positive quantities and vary γ, and write $P = P_\gamma$.

Clearly, P_0 is just the time $2\pi/\omega$ flow map of the unforced problem (2.2.6) and solution curves of the latter are invariant curves for P_0. In particular, the separatrices of the saddle point at (0, 0) for the flow are the invariant manifolds for the corresponding saddle point of P_0. Let us consider what happens to P_γ, and hence to the flow, as γ is increased from zero. We first describe the results of numerical solutions and Poincaré maps plotted from them. The results presented here are due to Ueda [1981a] (cf. [1981b]); for further results see Holmes [1979a].

For small values of γ, the two sinks of (2.2.6) at $(u, v) = (\pm 1, 0)$ become small ($\mathcal{O}(\gamma)$) attracting orbits of period $2\pi/\omega$ (period one for P_γ) and the saddle point becomes a saddle-type orbit. Thus P_γ continues to have three hyperbolic fixed points. As γ increases, the amplitude of the orbits, particularly the stable ones, grows continuously until, depending upon the precise values of δ and ω, a bifurcation occurs. Linearizing (2.2.6) at $(\pm 1, 0)$ we find that the unperturbed natural frequency, with $\delta = 0$, is $\sqrt{2}$. Moving out, the orbits surrounding $(\pm 1, 0)$ have successively longer periods, the periods tending to infinity as we approach the double homoclinic connection (Figure 2.2.3(a)), Locally, therefore, the oscillator near $(\pm 1, 0)$ behaves as a softening spring (Nayfeh and Mook [1979]), and if $\omega < \sqrt{2}$, a jump resonance occurs in which the small period 1 orbit is replaced by a relatively large period 1 orbit (Holmes [1979a]). If $\omega > \sqrt{2}$, and in particular if $\omega \approx 2\sqrt{2}$, a period 2 resonance can occur in which the fixed point of P_γ becomes unstable and undergoes a flip bifurcation in which a stable orbit of period $4\pi/\omega$ appears (Holmes and Holmes [1981]). Such jumps and the associated fold and flip bifurcations can be studied using the averaging results of Chapter 4.

In Figure 2.2.4(a) we show a pair of relatively large period 1 orbits ($\omega = 1 < \sqrt{2}$), projected onto the u, v plane, in addition to the associated fixed points of P_γ. As γ continues to increase, further bifurcations can occur in which such periodic points and the corresponding periodic orbits of the flow double their periods repeatedly. These accumulate at a point at which transition from periodic to apparently chaotic nonperiodic motion like that illustrated in Figure 2.2.2 occurs. Such cascades of period doubling bifurcations have been studied extensively and have many interesting universal properties (Feigenbaum [1978, 1980], Collet and Eckmann [1980]). We discuss some of this work in Chapters 5 and 6.

In Figures 2.2.4(b) and 2.2.5(a) we show typical orbits of a single point under the Poincaré map in this chaotic parameter regime. We note that these numerically observed "strange attractor" motions exist for relatively wide

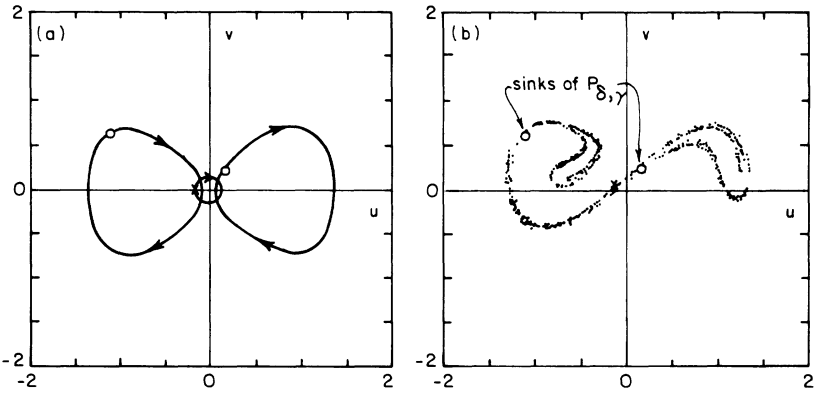

Figure 2.2.4. Orbits of the Duffing equation, $\delta = 0.25$, $\omega = 1.0$, $\gamma = 0.30$. (a) Two stable (○) and one saddle-type (×) periodic orbits, showing fixed points of P_γ; (b) the "strange attractor." Note that the stable periodic orbits (○) are close to marginal stability. Different numerical methods may yield unstable orbits.

sets of parameter values, that they can coexist with simple periodic motions, and that subharmonic motions are also observed in thin bands within the "strange attractor" region (cf. Figure 2.2.5(b)—see Holmes [1979a, Figure 7(e)] for a period 5 example). Considerably higher values of γ give rise to simple periodic motions of large amplitude once more; Figure 2.2.5(a).

Before offering a partial interpretation and explanation of these observations, we note that the irregular time history of Figure 2.2.2 displays considerable structure when viewed in a Poincaré map (Figures 2.2.4(b) and 2.2.5(a)) and that it appears to be genuinely nonperiodic—or at least to have period longer than any observation, as in the beam experiment. In Figure 2.2.6 we show power spectra of two such motions, which display the broad

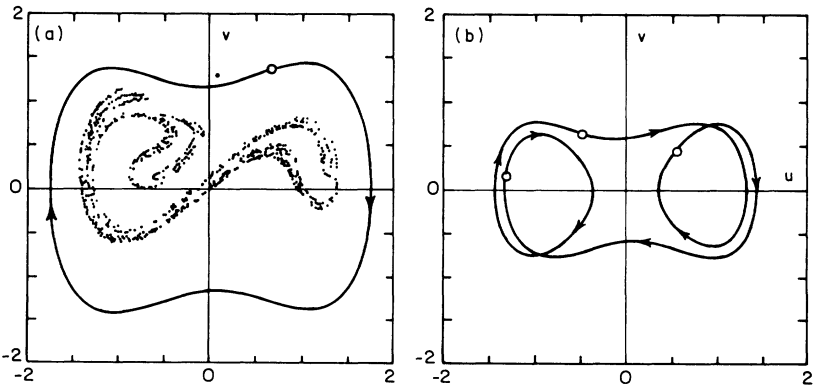

Figure 2.2.5. Orbits of the Duffing equation, $\omega = 1.0$, $\gamma = 0.30$. (a) Coexistence of a "strange attractor" and a large stable period 1 orbit, $\delta = 0.15$; (b) stable period 3 orbit, $\delta = 0.22$; the self-intersection is an artifact of the projection onto the (u, v)-plane.

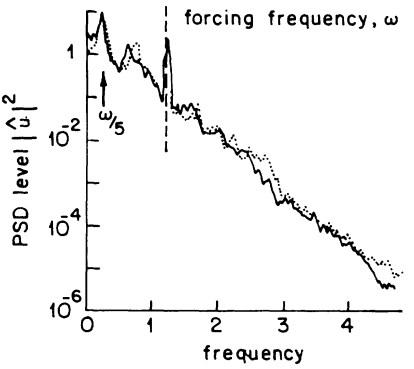

Figure 2.2.6. A power spectrum for the Duffing equation, $\omega = 1.19$, $\delta = 0.06$, $\gamma = 0.46$ ———, $\gamma = 0.57$ ····· (from Holmes [1979a]).

frequency content of the Fourier transform $\hat{u}(\omega)$ of $u(t)$. Note the presence of peaks at the forcing frequency and some of its subharmonics.

A major key to understanding these results lies in the analysis of the invariant manifolds of the saddle point of P_γ near (0, 0). We denote this point as p and its stable and unstable manifolds as $W^s(p)$, $W^u(p)$. As already noted, $W^s(p)$ and $W^u(p)$ for $\gamma = 0$ are simply the saddle separatrices of Figure 2.2.3(b) (cf. Figure 2.2.7(a)). The Poincaré map P_0 has three hyperbolic fixed points and the manifolds do not intersect, and therefore we can immediately conclude that P_γ for small γ is topologically equivalent to P_0, since P_0 is structurally stable. The numerical observations illustrate this (Figure 2.2.7(b)). As γ increases, however, the manifolds can and do become tangent and subsequently intersect transversely; Figure 2.2.7(c), (d) (see Figure 4.5.3(b) for a quadratic contact). The partial plots of $W^s(p)$ and $W^u(p)$ of Figure 2.2.7 are produced by iterating a number of points defining a short segment of $W^s(p)$ (or $W^u(p)$) near p under P_γ^{-1} (or P_γ). This *global* bifurcation occurs in addition to, and independently of, the local period doubling or jump (fold) bifurcations of fixed points referred to above.

In Chapter 4 we shall see how to compute the location of such global homoclinic bifurcations for systems like (2.2.8), in the case that γ, δ are small and the system is close to an integrable Hamiltonian one. At the same time we shall be able to find subharmonic motions which bifurcate from the continuous families of periodic orbits of Figure 2.2.3(a).

Once the manifolds intersect, we have *transversal homoclinic orbits*, and in Chapter 5 we shall see that their presence implies the existence of a complicated nonwandering Cantor set which possesses infinitely many unstable periodic orbits of arbitrary long period as well as bounded nonperiodic motions (also see Section 2.4.4, below). Moreover, for certain parameter values near those at which homoclinic tangencies occur, the work of Newhouse [1979, 1980] shows that infinite sets of *stable* periodic orbits (called Newhouse sinks) exist. We shall discuss these in Chapter 6. All this complex

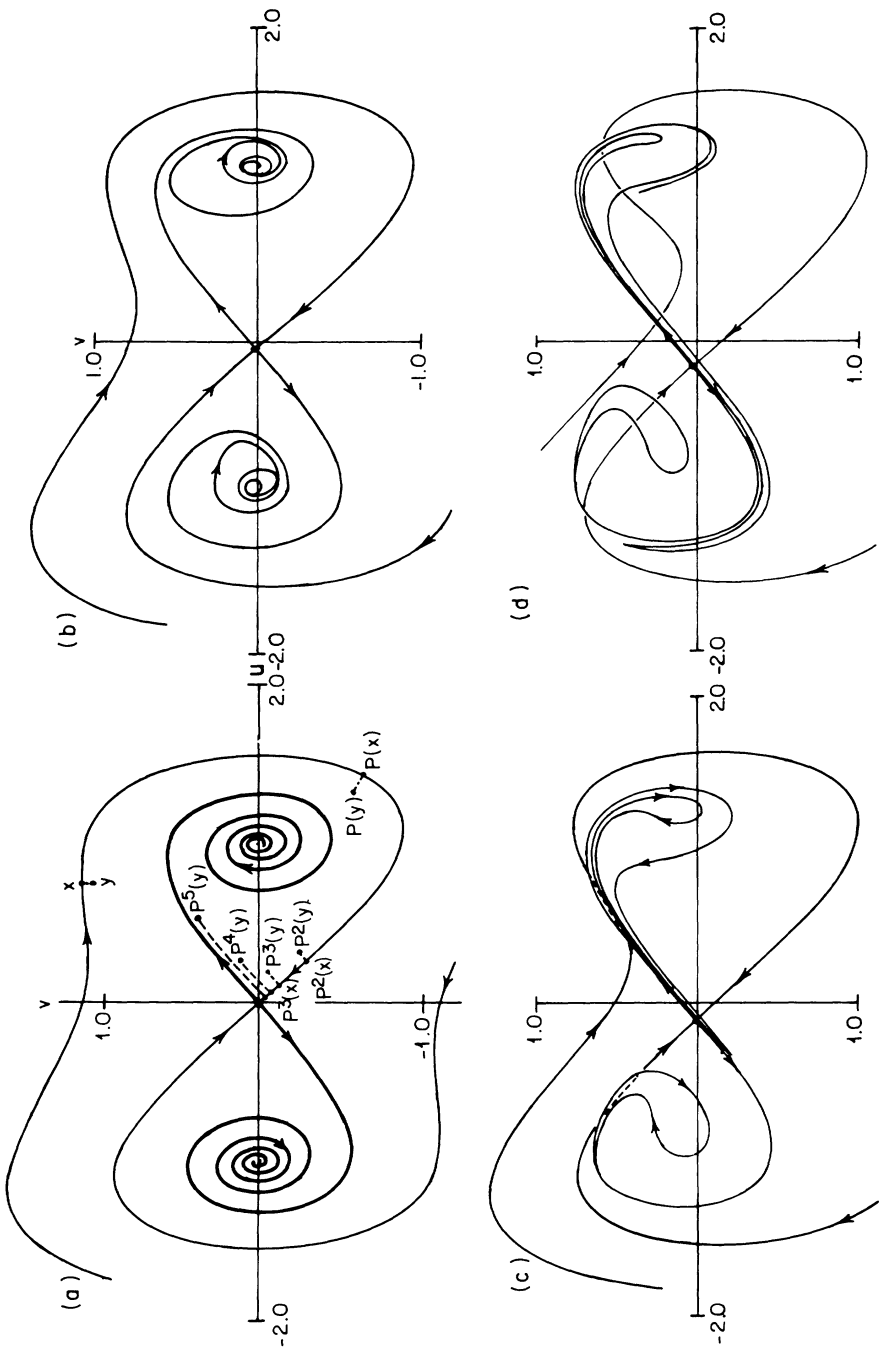

Figure 2.2.7. The Poincaré maps for the Duffing equation (2.2.8), $\delta = 0.25$, $\omega = 1.0$. (a) $\gamma = 0$; (b) $\gamma = 0.10$; (c) $\gamma = 0.20$; (d) $\gamma = 0.30$. Typical orbits shown in (a), and attracting set marked as a heavy curve.

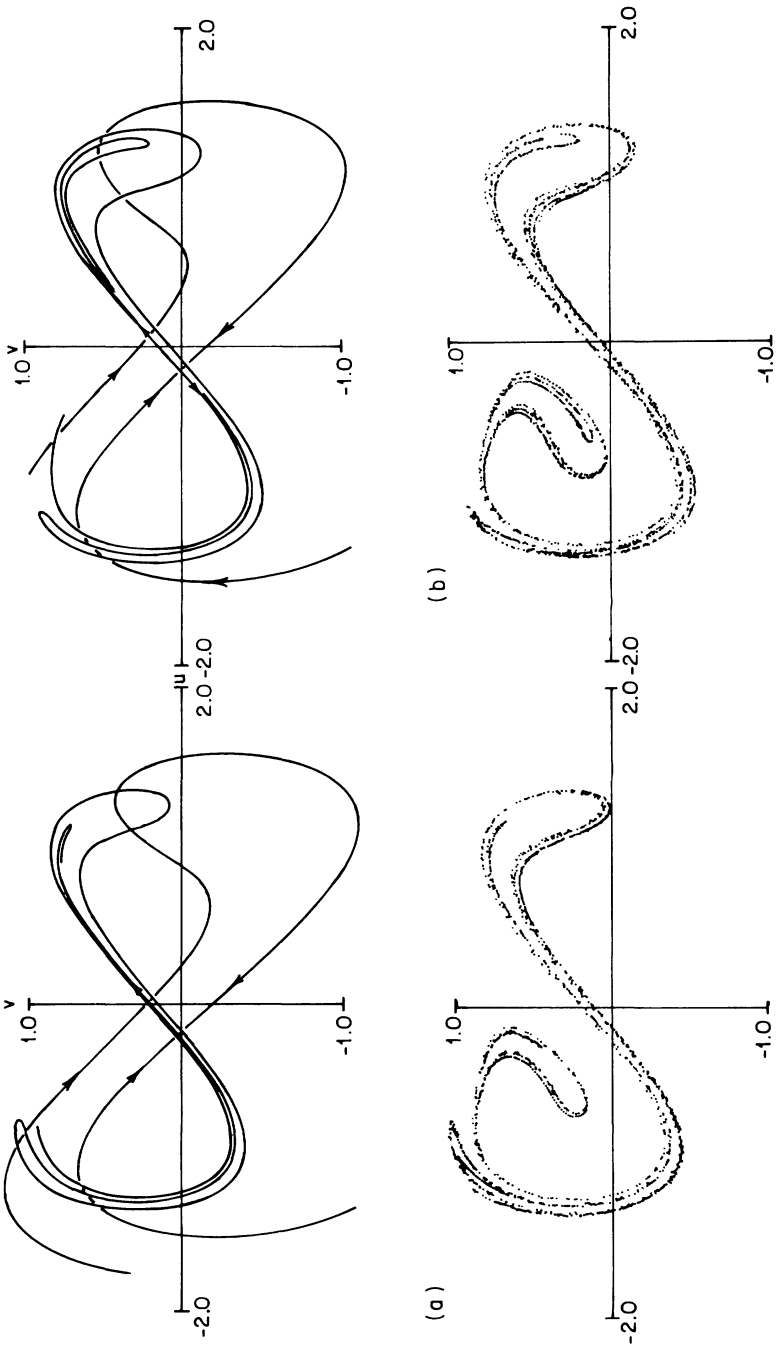

Figure 2.2.8. Invariant manifolds and attracting sets for the Duffing equation (2.2.8), $\omega = 1.0$. (a) $\delta = 0.25$; $\gamma = 0.40$; (b) $\delta = 0.20$, $\gamma = 0.30$.

behavior contributes to the attracting set, the structure of which we now turn to.

As noted above, a closed disc $D \subset \Sigma$ can be found such that $P_\gamma^n(D) \subset D$ for $n > 0$, and we can again define the closed attracting set as

$$A_\gamma = \bigcap_{n \geq 0} P_\gamma^n(D).$$

Comparing numerically obtained plots of the strange attractors with the unstable manifold of the saddle point, $W^u(p)$, we are led to the conjecture that this set A_γ is equal to the closure of the unstable manifold; cf. Figure 2.2.8. A_γ is certainly of zero area, since the flow of (2.2.8) contracts volume uniformly, because the divergence of the vector field is

$$\frac{\partial}{\partial u}(v) + \frac{\partial}{\partial v}(u - u^3 - \delta v + \gamma \cos \omega\theta) + \frac{\partial}{\partial \theta}(1) = -\delta < 0, \tag{2.2.9}$$

and hence $\det |DP_\gamma| = e^{-2\pi\delta/\omega} < 1$.

For small γ our conjecture is proved by noting that all orbits $\{P_\gamma^n(y)\}$ of $y \in D$ approach one of the sinks except those of points $x \in W^s(p)$, which approach p. A_γ therefore contains the sinks and the saddle. To see that all points in A_γ lie in the closure of $W^u(p)$, consider any curve C joining a point $x \in W^s(p)$ to a point $y \in D$. (Figure 2.2.7(a)). As $n \to \infty$, the endpoints of $P^n(C)$ approach the saddle and the sink, as do all points on C except those arbitrarily close to $P^n(x)$. Thus $P^n(C)$ approaches a component of $W^u(p)$, as claimed.

The situation is more complicated in the presence of homoclinic intersections. Even if our conjecture is true, the set A_γ may contain proper subsets such as the Newhouse sinks which are attracting. What is of interest here is that, unlike the van der Pol oscillator; there are *no* low period sinks for certain parameter ranges. We conjecture that, for each integer $N < \infty$, there is an open set of parameter values γ, δ, ω for which P_γ has no attracting periodic orbits of period less than N. Such attractors are effectively unobservable for even moderately large values of N because the characteristic width of their domains of attraction decreases dramatically (in certain cases like e^{-N} (Greenspan and Holmes [1982])) and physical or numerical noise becomes dominant at these scales. Thus the asymptotic behavior of trajectories within A_γ appears complicated. In some regimes there appear to be trajectories which are dense in A_γ. There is a substantial theoretical question as to whether this "strange attractor" of the Duffing equation is an artifact of the noise and is absent in the ideal deterministic system. We discuss in a general context the issue of the existence of strange attractors in Chapters 5 and 6.

In Section 2.4.4 we discuss a nonlinear map which displays behavior similar in many aspects to that of the Duffing Poincaré map, and in which the structure of the attracting set can be displayed more readily.